The Visual Computer (2023) 39:297–318
https://doi.org/10.1007/s00371-021-02330-z

ORIGINAL ARTICLE

Adaptive tri-plateau limit tri-histogram equalization algorithm for digital image enhancement

Abhisek Paul[1]

Accepted: 10 October 2021 / Published online: 2 November 2021

Abstract
Histogram equalization (HE) is one of the most important techniques for contrast enhancement of digital images. Conventional HE methods persuade excessive enhancement, unnatural artifacts and brightness transform resulting abnormal and unusual appearance. To solve such problems, a novel tri-plateau limit-oriented tri-histogram equalization technique is suggested for digital image enhancement, where histogram of the input image is initially separated in three sub-histograms using separation threshold parameters. Next, plateau limit criteria for sub-histograms are formulated using the average of the mean and the median of each sub-histogram, and subsequently, a redistributed parameter is calculated and merged with each sub-histogram to restrict over-enhancement. Finally, modified sub-histograms are equalized separately and the enhanced image is produced by incorporating the images accomplished by the transformation function. Experimental results demonstrate that the proposed technique efficiently enhances the contrast of images, while visual quality assessments and quantitative measures, like average information content (AIC), feature similarity index measure (FSIM), multi scale structural similarity index measure (MS-SSIM), visual saliency-induced index (VSI), and gradient magnitude similarity deviation (GMSD) effectively validate the superiority of the proposed algorithm with respect to the other traditional state-of-the-art HE methods.

Keywords Histogram equalization · Plateau limit · Average information content · Contrast enhancement

1 Introduction

Image enhancement is one of the most important prerequisites for facilitating image in multimedia information retrieval [1–3]. In recent, different types of image enhancement mechanisms are suggested, such as image de-noising [4], image de-hazing [5–7], image sharpening [8], image de-blurring [9], image fog removal [10], image filtering [11], histogram stretching [12], image shadow removal [13], image smoothing [14,15], histogram equalization [16–20]. Histogram equalization (HE) [16] is one of the simplest and quickest methods in the area of brightness conservation and contrast improvement of digital images, where using the probability density function of the input histogram, image intensity is mapped to a dynamic range for contrast improvement of digital images [16]. However, a variety of HE methods are utilized for enhancing different types of images such as, underwater image [21], infrared (IR) image [22,23], magnetic resonant imaging (MRI) [24], computed tomography (CT) image [25], endoscopic image [26], heritage image [27], satellite image [28].

Basically, HE shifts the mean intensity of the image abruptly and causes extra artifacts. However, to diminish such occurrences bi-HE oriented methods like, brightness preserving bi-HE (BBHE) [29], dualistic sub-image HE (DSIHE) [30], minimum mean brightness error bi-HE (MMBEBHE) [31] are presented, where input histogram is divided in two different sub-histograms using respective sub-histogram separation criteria and equalized each sub-histogram independently. Later, recursive mean separate HE (RMSHE) [32], recursive sub-image HE (RSIHE) [33] schemes are suggested, where histogram is divided using a recursive level r. Initially, when $r = 1$ histogram separation is done using the mean and the median intensity of the input image for RMSHE and RSIHE. Subsequently, BBHE and DSIHE methods are applied in two sub-histograms for RMSHE and RSIHE, respectively, and each sub-histogram is equalized independently. Here, when $r = 2$, RMSHE and RSIHE are divided

✉ Abhisek Paul
abhisekpaul13@gmail.com

[1] Department of Computer Science and Engineering, National Institute of Technology, Agartala, India

into four sub-histograms. In both of the methods, resultant output produces miscellaneous artifacts.

In general, above-mentioned methods could not restrict over-enhancement outcome. So, to restrict over-enhancement, plateau limit (PL) or clip limit (CL) criteria for histogram are recommended in bi-HE with a PL (BHEPL) [34], where histogram is spit in two sub-histograms and PL mechanism is applied in two sub-histograms before final independent sub-histogram equalization. Chen and Nor [35] proposed dynamic quadrants HE using plateau limit (DQHEPL) method, where PL of four sub-histograms is based on the mean of each sub-histogram, respectively. Then, modified histograms are equalized autonomously. Similarly, in [36] double plateau limit-based HE method is suggested, where plateau limits are computed using multiple coefficients using input histogram but could not enhance low-light or degraded images efficiently. Another bi-HE-based method is proposed in [18], where probability density values of an input histogram are selected for bisection threshold parameter. Here, degradation of output is observed for dim and low-contrast images. Modified histogram clipping using the difference of histogram bins (MCDHB) is proposed in [37], where 15% of threshold parameter is redistributed with clipped histogram, and difference of the original histogram and the histogram of the conventional HE is taken into consideration for six types of adaptive PL criteria before the final HE process.

In recent, various quad-histogram-based HE methods are proposed [38–40], where input histograms are subdivided in four sub-histograms, using respective criteria and finally equalized independently. These quad-based HE methods provide brightness preservation of the input image quite proficiently, but could not enhance degraded or low-contrast images very efficiently. In [20], combination of low dynamic range (LDR) HE and Haar wavelet transform (HWT) is used for local and global contrast enhancement of images. Here, special inverse operation is done for regulating extra enhancement in the construction phase. Recursion-oriented multi-histogram clipping HE method is suggested in [41], where histogram is separated in two or more sub-histogram and six types of histogram clipping are considered for brightness preservation and contrast enhancement. These types of multi-plateau and multi-histogram equalization normally increase computational complexity. Histogram division is an important issue in multi-histogram equalization; in most of the above-discussed methods, separation of histogram is done in imbalanced range, such as over-extended or small-spanning. To overcome such issue, Lin et al. [42] uttered statistic separate tri-HE technique (SSTHE), where input histogram is split into clusters of three sub-histograms using the mean brightness and the standard deviation (SD) of the image, then each sub-histograms are equalized independently. Here, SSTHE does not include clipping of histogram, and subsequently, over enhancement in the output image can be observed.

In [43], PL-based tri-HE method (PLTHE) is suggested using the SD of the image, where middle sub-histogram acquires maximum histogram pits and the average of the mean and the median of the histogram is used as a plateau limit, and finally, sub-histograms are equalized separately, whereas first and the last sub-histograms often remain unclipped, and therefore, over-enhancement can be visible in the output image. In [44], mean or median-based triple dynamic clipped HE (TDCHEM) is proposed, where the initial separation of the input histogram is made of two parts using the median or the mean of the input image. Then, the range of first sub-histogram is denoted from minimum input image intensity to 66% of entire number of pixels in the upper sub-histogram, and the range of second sub-histogram is indicated from first separation point to 33% of entire number of pixels in the lower sub-histogram, and the range of third sub-histogram is indicated from second separation point to maximum level of input image intensity. However, the output of this method creates unwanted artifacts and over-enhancement due to the mapping of partitions into dynamic ranges abruptly. Zarie et al. [45] proposed SD-based triple clipped dynamic HE method (TCDHESD), where histogram of input image is separated into three pieces with nearly equal amount of pixels based on the SD of the input image, and subsequently, the PL of each sub-histogram is done using the mean of each sub-histogram. In TCDHESD, the desired output become slightly over-enhanced, and few visible artifacts are observed due to mapping of sub-histograms in new dynamic ranges.

Motivated from the various tri-HE base methods, specially PLTHE method and various PL criteria of histogram as discussed above, in this paper, we have suggested a novel tri-plateau limit tri-HE method, where input histogram is separated in three sub-histograms using separation threshold parameter, and individual sub-histogram plateau limit criteria is included to compute tri-plateau sub-histograms. Later, redistribution of clipped portion is done to sub-histogram, and finally, modified sub-histograms are equalized separately to achieve the enhanced output.

Contributions of this paper are given as follows:

1. Histogram of the input image is divided in three sub-histograms, and histogram division mechanism is prepared using threshold parameters, which are generated using standard deviation of the input image. In PLTHE [43] method, for most of the images, the initial and the last sub-histograms, i.e., two boundary sub-histograms remain very small and negligible, because calculation

of threshold parameters does not include the maximum and the minimum intensity of the image. Here, in this proposed method, the maximum and the minimum intensity of the image is considered for two boundary sub-histogram generation.

2. In histogram modification criteria, sub-histograms are clipped using individual plateau limit criteria, where the average of the mean and the median of the individual sub-histogram is considered as plateau limit. Clipped sub-histograms are redistributed using redistribution parameter, which is formulated using the clipped pixels of the histogram.
3. In performance analysis, various recent trend HE methods are preferred, out of which tri-HE methods, like SSTHE [42], PLTHE [43], TDCHEM [44], and TCDHESD [45], are also considered. For quantitative assessment, average information content (AIC) [46], feature similarity index metric (FSIM) [47], multi-scale structural similarity index measure (MS-SSIM) [48], visual saliency induced index (VSI) [49], and gradient magnitude similarity deviation (GMSD) [50] are considered. Images with diverse image features from various well-known data-sets, like USC-SIPI image data-set [51], Kodak image data-set [52], CSIQ image data-set [53], and Berkeley image data-set [54] are selected. Quantitative results of various HE methods for more than 550 images are represented as graphical and tabular forms considering image data-sets [52–54] .

The remaining part of this paper is organized as follows: Sect. 2 describes the proposed adaptive tri-plateau limit tri histogram equalization method, Sect. 3 demonstrates experimental results and analysis, and finally, Sect. 4 represents conclusions.

2 Proposed method

Conventional histogram equalization amplifies the contrast of an image by stretching the histogram as wide as possible to a specified range. For a given image I, the histogram $H(i)$ for intensity level i is defined as

$$H(i) = n_i \quad for\ i = 0, 1, 2, ...(L-1), \tag{1}$$

where L is the maximum range of gray level, (256 for an 8-bit image, 0 to 255). Here, n_i is the number of pixels of the image whose intensity level is i. Here, N is the total number of pixels in the image, and it is shown as:

$$N = \sum_{i=0}^{L-1} H(i). \tag{2}$$

Figure 1 demonstrates partition and modification mechanism of input histogram for the proposed method.

Initially, the input histogram is split into three sub-histograms using two threshold parameters X_L and X_U, which are given as follows:

$$\begin{cases} X_L = X_0 + SD \\ X_U = X_m - SD, \end{cases} \tag{3}$$

where SD is the standard deviation [42] of the input image, and X_0 and X_m are the minimum and the maximum intensities of the input image, respectively. Three sub-histograms are denoted as H_L, H_M, and H_U, and their corresponding range of intensities is from 0 to X_L, X_L+1 to X_U, and X_U+1 to $L-1$, respectively. However, loss of contact between two sub-histograms can create artifacts, so lower sub-histogram ends in X_L intensity and middle sub-histogram starts in

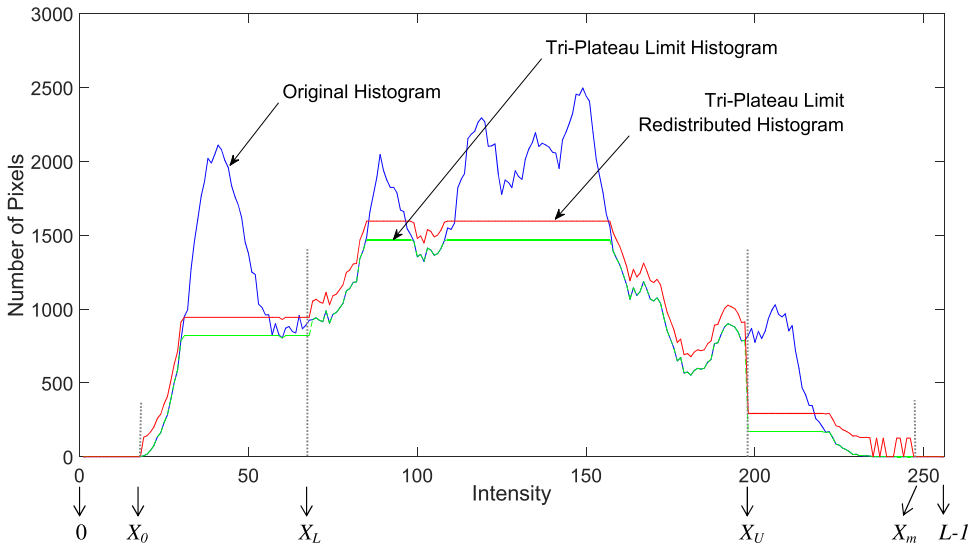

Fig. 1 Partition and modification criteria of histogram for the proposed algorithm

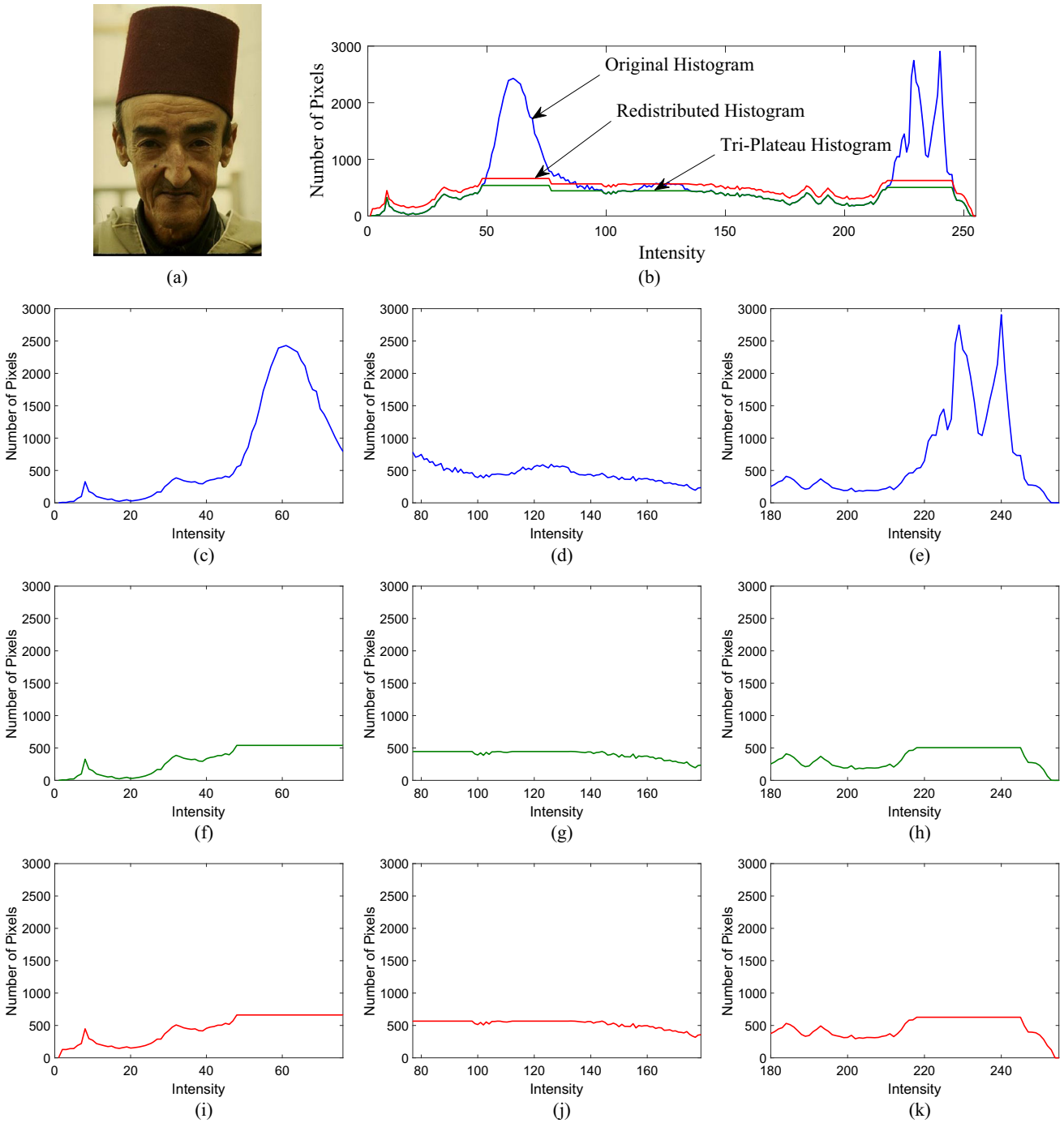

Fig. 2 Example of the proposed method: (**a**) Original image, (**b**) Histogram modification for the proposed method, (**c**–**e**) Three sub-histograms for the proposed method, (**f**–**h**) Clipped sub-histograms, and (**i**–**k**) Redistributed sub-histograms

$X_L + 1$ intensity. In the same way, middle sub-histogram ends in X_U intensity and upper sub-histogram starts in $X_U + 1$ intensity, respectively.

Figures 2 and 3 clearly illustrate the proposed method graphically, where the input image, histogram of the input image, histogram division, sub-histogram modification, probability density function, cumulative probability density function, transformation function for input-output mapping curve, and output image are shown.

To restrict over-enhancement, most of the HE-based methods use the mean or the median as a plateau limit. Basically, the mean and the median are alike in symmetrical data-distribution. If the data are not symmetrically distributed (positively skewed/negatively skewed), then the mean and

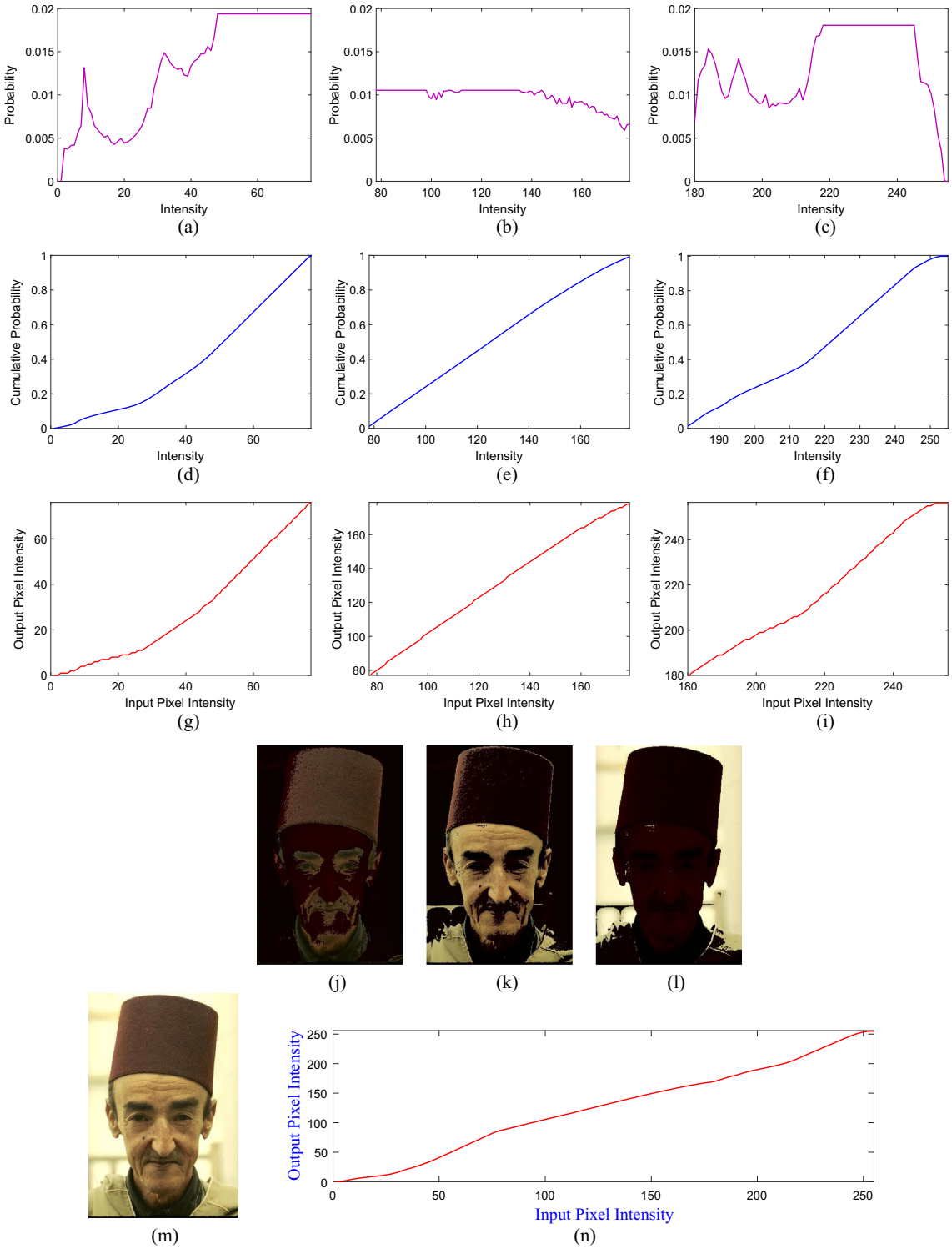

Fig. 3 (Fig. 2 continued): for three sub-histograms (**a**–**c**) Probability distributions, (**d**–**f** Cumulative probability distributions (**g**–**i**) Input-output mapping curves, (**j**–**l**) Three sub-images from mapping curves, (**m**) Output image, and (**n**) Transformation function (merging three mapping curves) for the proposed method

median are not equal. This proposed method gives the flexibility to deal with these variations in the data-distribution, and it is achieved by the average of the median and the mean of the individual sub-histogram for choosing the plateau limit threshold parameters. These parameters are formulated as

$$\begin{cases} PL_L = \dfrac{mean[H_L(i)] + median[H_L(i)]}{2} & for \quad 0 \le i \le X_L \\ PL_M = \dfrac{mean[H_M(i)] + median[H_M(i)]}{2} & for \quad X_L + 1 \le i \le X_U \\ PL_U = \dfrac{mean[H_U(i)] + median[H_U(i)]}{2} & for \quad X_U + 1 \le i \le L - 1. \end{cases} \tag{4}$$

Plateau limit sub-histograms are generated using plateau limit threshold parameters, and these modified sub-histograms are computed as

$$\begin{cases} H_{PL}(i) = \begin{cases} PL_L & \text{if } H(i) \ge PL_L \\ H(i) & \text{if } H(i) < PL_L \end{cases} & for \quad 0 \le i \le X_L \\ H_{PM}(i) = \begin{cases} PL_M & \text{if } H(i) \ge PL_M \\ H(i) & \text{if } H(i) < PL_M \end{cases} & for \quad X_L + 1 \le i \le X_U \\ H_{PU}(i) = \begin{cases} PL_U & \text{if } H(i) \ge PL_U \\ H(i) & \text{if } H(i) < PL_U \end{cases} & for \quad X_U + 1 \le i \le L - 1. \end{cases} \tag{5}$$

Plateau limit sub-histograms are combined as

$$H_{TPL} = H_{PL} \cup H_{PM} \cup H_{PU}. \tag{6}$$

Next, the total number of clipped pixels can be represented as the histogram, H_S and this is formulated as

$$H_S(i) = H(i) - H_{TPL}(i) \qquad for \quad 0 \le i \le L - 1. \tag{7}$$

In this proposed approach, a redistributed parameter is merged with plateau limit sub-histograms to cut down over-enhancement and provide clear visualization, and this redistributed parameter is calculated as

$$R = \frac{mean[H_S] + median[H_S]}{2}. \tag{8}$$

This proposed method also provides the flexibility to the redistribution parameter. The mean or the median of the clipped portion is not taken directly as a redistributed parameter. Here, it is achieved by the average of the median and the mean of the clipped portion from the input histogram.

Now, using redistributed parameter, redistributed sub-histograms are computed as

$$\begin{cases} H_{RL}(i) = \begin{cases} H_{PL}(i) & \text{if } H_{PL}(i) < 1 \\ H_{PL}(i) + R & \text{if } H_{PL}(i) \ge 1 \end{cases} & for \quad 0 \le i \le X_L \\ H_{RM}(i) = \begin{cases} H_{PM}(i) & \text{if } H_{PM}(i) < 1 \\ H_{PM}(i) + R & \text{if } H_{PM}(i) \ge 1 \end{cases} & for \; X_L + 1 \le i \le X_U \\ H_{RU}(i) = \begin{cases} H_{PU}(i) & \text{if } H_{PU}(i) < 1 \\ H_{PU}(i) + R & \text{if } H_{PU}(i) \ge 1 \end{cases} & for \; X_U + 1 \le i \le L - 1. \end{cases} \tag{9}$$

Here, redistributed parameter is merged with non-empty histogram bins. Generally, for low contrast image, a very small amount of non-empty histogram bins are present. If redistributed parameter is merged with all histogram bins comparatively less enhanced image is formed. Whereas, if non-empty histogram bins are selected for merging the redistributed parameter than comparatively well enhanced image can be achieved. A demonstration of such phenomenon is shown in Fig. 4

Probability density functions (PDFs) of redistributed sub-histograms are PD_L, PD_M and PD_U, which are computed as

$$\begin{cases} PD_L(i) = \frac{H_{RL}(i)}{N_L} & for \quad 0 \le i \le X_L \\ PD_M(i) = \frac{H_{RM}(i)}{N_M} & for \quad X_L + 1 \le i \le X_U \\ PD_U(i) = \frac{H_{RU}(i)}{N_U} & for \quad X_U + 1 \le i \le L - 1. \end{cases} \tag{10}$$

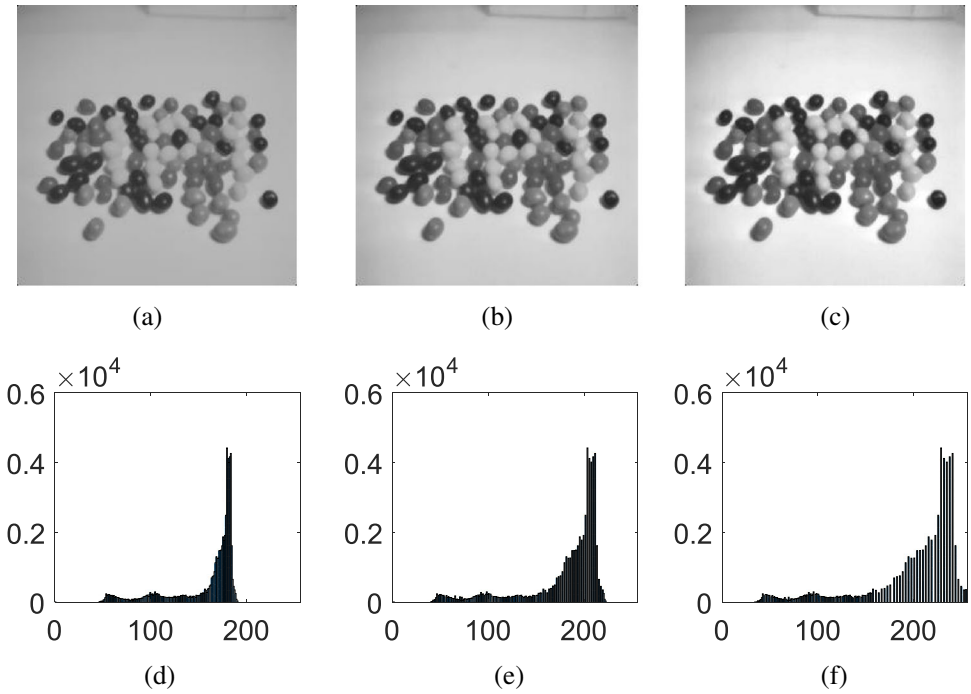

Fig. 4 Example of the effect of adding redistribution parameter. (**a**) low contrast input image, (**b**) output of the proposed method, where the redistribution parameter is added with all histogram bins, (**c**) output of the proposed method, where the redistribution parameter is added only with non-empty histogram bins. (**d**–**f**) histogram of (**a**–**c**), respectively, where vertical axis indicates number of pixels and horizontal axis indicates image intensity

where N_L, N_M, and N_U are total number of pixels in redistributed sub-histograms H_{RL}, H_{RM}, and H_{RU}, respectively. Finally, the transformation function is calculated as

$$T_F(i) = \begin{cases} X_L \times \sum_{i=0}^{X_L} PD_L(i) & for \quad 0 \le i \le X_L \\ (X_L+1) + (X_U - (X_L+1)) \times \sum_{i=X_L+1}^{X_U} PD_M(i) & for \quad X_L+1 \le i \le X_U \\ (X_U+1) + ((L-1) - (X_U+1)) \times \sum_{i=X_U+1}^{L-1} PD_U(i) & for \quad X_U+1 \le i \le L-1. \end{cases} \tag{11}$$

Transformation function T_F represents the desired mapping function for the proposed algorithm. Here, variable k is used to calculate cumulative probability till k-th intensity.

Detail steps of the proposed method are given as follows:

1. Histogram, $H(i)$ is formed from the input image.
2. Histogram separation threshold parameters, X_L and X_U, are calculated using Eq. 3.
3. Three sub-histograms, H_L, H_M, and H_U are formed using histogram separation threshold parameters, where corresponding ranges of intensities for sub-histograms are from 0 to X_L, X_L+1 to X_U, and X_U+1 to $L-1$, respectively.
4. Plateau limit parameters, PL_L, PL_M and PL_U, are calculated for three sub-histograms using Eq. 4.
5. Plateau limit sub-histograms, H_{PL}, H_{PM} and H_{PU}, are formulated as shown in Eq. 5.
6. Plateau limit sub-histograms are combined and subtracted from the original histogram to generate the histogram of clipped pixels using Eqs. 6 and 7, where H_{TPL} is the combination of plateau sub-histograms and H_S is the histogram of clipped pixels.
7. Redistribution parameter, R, is calculated using Eq. 8.
8. Modified sub-histograms are formulated using the redistribution parameter, as shown in Eq. 9.
9. After that probability density functions (PDFs) of modified sub-histograms are given as PD_L, PD_M, and PD_U, as shown in Eq. 10.
10. Next, transformation function T_F is formulated using Eq. 11 for the proposed method, where cumulative PDFs are used for respective sub-histogram equalization. Finally, image intensities are rounded to the nearest integer.

3 Experimental results and analysis

To evaluate performance of the proposed method, state-of-the-art algorithms like SSTHE [42], DQHEPL [35], MCDHB [37], PLTHE [43], TDCHEM [44], and TCDHESD [45] are compared. Quantitative and qualitative assessments are accomplished using MATLAB environment with windows 10 operating system, Intel core i5 (3.6GHz), and 8 GB RAM. Here, gray-scale images are taken directly for experiments, whereas for color images, the input image is converted from RGB to YUV color space. Different HE algorithms are applied only on the Y component, and quantitative results of different HE methods are applied on Y component only, where U and V color components are unchanged. After applying any HE technique to Y component, YUV to RGB

conversion is done [16]. Images are selected from various image data-sets, like USC-SIPI image data-set [51], Kodak image data-set [52], CSIQ image data-set [53], and Berkeley image data-set [54], where quantitative results of images from three data-sets [52–54] are symbolized in graphical and tabular forms.

3.1 Quantitative assessment

In quantitative assessment, quantitative measures like AIC [46], FSIM [47], MS-SSIM [48], VSI [49], and GMSD [50] are considered. In recent, these quantitative measures are highly used in different image enhancement methods [55–59] for quantitative evaluations.

3.1.1 AIC

AIC or average information content represents total information content in an image [46]. The AIC is defined as:

$$AIC = -\sum_{i=0}^{L-1} P(i)\log_2 P(i), \tag{12}$$

where probability density function of an image is $P(i)$ at intensity point i and L is the maximum image intensity level. Larger value of AIC indicates more information content.

3.1.2 FSIM

Feature similarity index metric or FSIM demonstrates the overall similarity between the input image m_1 and the enhanced image m_2. Phase congruence for m_1 and m_2 is described as P_1 and P_2, respectively. $S_{LS}(i)$ provides the local similarity of $m_1(i)$ and $m_2(i)$ at i pixel position. Maximum of $P_1(i)$ and $P_2(i)$ is denoted as $P_m(i)$. Entire image in spatial domain is denoted as Ω. FSIM outcome between m_1 and m_2 is formulated as:

$$FSIM = \frac{\sum_{i\subset\Omega} S_{LS}(i).P_m(i)}{\sum_{i\subset\Omega} P_m(i)}. \tag{13}$$

FSIM output is between 0 and 1, and higher value indicates greater enhancement.

3.1.3 MS-SSIM

Multi-scale structural similarity index measure or MS-SSIM is suggested by Wang et al. [48]. General structural similarity index [48] between signal x and y is as follows:

$$GSSIM = [l(x,y)]^{\alpha}[c(x,y)]^{\beta}[s(x,y)]^{\gamma}, \tag{14}$$

where luminance, contrast, and structure factors of the image are denoted as $[l(x,y)]$, $[c(x,y)]$, and $[s(x,y)]$, respectively, where α, β, and γ are used to define the relative importance of three components. MS-SSIM is defined as follows:

$$MS-SSIM = [l_M(x,y)]^{\alpha M}.\prod_{j=1}^{M}[c_j(x,y)]^{\beta j}[s_j(x,y)]^{\gamma j}. \tag{15}$$

Here, $[c_j(x,y)]$ and $[s_j(x,y)]$ are computed at j-th scale and only luminance comparison $[l(x,y)]$ is calculated in M scale as shown in Eq. (15). Larger value of MS-SSIM confirms superior image quality.

3.1.4 VSI

Visual saliency index or VSI of input image m_1 and output image m_2 is described as V_{s1} and V_{s2}, respectively. $S_{LS}(i)$ provides the local similarity of $m_1(i)$ and $m_2(i)$ at i pixel position. Maximum of $V_{s1}(i)$ and $V_{s2}(i)$ is denoted as $V_{mx}(i)$. Entire image in spatial domain is denoted as Ω. Higher value of VSI indicates greater enhancement. VSI outcome between m_1 and m_2 is formulated as:

$$VSI = \frac{\sum_{i\subset\Omega} S_{LS}(i).V_{mx}(i)}{\sum_{i\subset\Omega} V_{mx}(i)}. \tag{16}$$

3.1.5 GMSD

Xue et al. [50] established an image quality measurement metric called gradient magnitude similarity deviation (GMSD). Standard deviation of gradient magnitude similarity (GMS) at each pixel of an image is called as GMSD. In the mathematical formulation, M_{m1} and M_{m2} are the magnitudes of gradients of the input image m_1 and the distorted image m_2, respectively, at i pixel location, where C is a positive constant. Mean of GMS (GMSM) is used to formulate GMSD with total pixel number P_X as shown in Eqs. (17) and (18). Equation (19) gives the calculation for GMSD.

$$GMS(i) = \frac{2M_{m1}(i).M_{m2}(i)+C}{M_{m1}^2(i).M_{m2}^2(i)+C}. \tag{17}$$

$$GMSM = \frac{1}{P_X}\sum_{i=1}^{P_X}(GMS(i))^2. \tag{18}$$

$$GMSD = \left(\frac{1}{P_X}\sum_{i=1}^{P_X}(GMS(i)-GMSM)^2\right)^{1/2}. \tag{19}$$

Lower value of GMSD explains less distortion in image quality so that the visual perception is better.

Tables 1 and 2 represent output of various quantitative metrics for different HE methods, where fifteen test images

Table 1 Performance evaluation of contrast enhancement algorithms

Image	Metric	SSTHE 2009 [42]	DQHEPL 2010 [35]	MCDHB 2019 [37]	PLTHE 2018 [43]	TDCHEM 2018 [44]	TCDHESD 2019 [45]	Proposed
Hawks	AIC	5.649	5.653	5.409	5.754	5.688	5.689	**5.774**
	FSIM	0.876	0.865	0.816	0.942	0.829	0.848	**0.981**
	MS-SSIM	0.921	0.867	0.651	0.888	0.774	0.853	**0.972**
	VSI	0.939	0.965	0.965	0.988	0.963	0.9867	**0.995**
	GMSD	0.118	0.079	0.119	0.038	0.098	0.098	**0.016**
Buffalo	AIC	5.104	5.121	5.021	5.243	5.0115	5.172	**5.260**
	FSIM	0.716	0.610	0.419	0.688	0.573	0.648	**0.894**
	MS-SSIM	0.718	0.599	0.312	0.659	0.634	0.597	**0.890**
	VSI	0.881	0.853	0.750	0.912	0.837	0.881	**0.976**
	GMSD	0.227	0.200	0.234	0.146	0.197	0.203	**0.057**
Moon	AIC	4.502	4.472	3.980	4.702	4.668	4.664	**4.714**
	FSIM	0.788	0.797	0.521	0.830	0.731	0.792	**0.938**
	MS-SSIM	**0.928**	0.837	0.541	0.745	0.707	0.806	0.911
	VSI	0.948	0.936	0.781	0.943	0.895	0.923	**0.986**
	GMSD	0.094	0.142	0.246	0.142	0.187	0.162	**0.059**
Tiffany	AIC	6.449	6.535	6.283	**6.582**	6.517	6.609	6.584
	FSIM	0.856	0.921	0.808	0.885	0.908	0.886	**0.945**
	MS-SSIM	0.843	0.913	0.760	0.849	**0.893**	0.862	0.924
	VSI	0.933	0.966	0.935	0.963	0.962	0.956	**0.985**
	GMSD	0.201	0.103	0.114	0.094	0.111	0.125	**0.046**
Lady	AIC	5.251	5.260	5.217	5.477	5.462	5.461	**5.502**
	FSIM	0.876	0.942	0.609	0.952	0.878	0.971	**0.973**
	MS-SSIM	0.920	0.949	0.559	0.961	0.914	0.974	**0.980**
	VSI	0.974	0.985	0.853	0.989	0.974	0.990	**0.991**
	GMSD	0.076	0.054	0.251	0.042	0.085	0.027	**0.024**
Child	AIC	6.946	7.015	6.841	**7.047**	7.026	7.037	7.013
	FSIM	0.924	0.945	0.903	0.977	0.913	0.912	**0.981**
	MS-SSIM	0.936	0.953	0.888	0.976	0.906	0.905	**0.982**
	VSI	0.972	0.981	0.970	0.993	0.969	0.970	**0.995**
	GMSD	0.065	0.040	0.071	**0.012**	0.048	0.052	0.015
Gate	AIC	6.948	7.051	**7.093**	7.070	7.083	7.062	7.041
	FSIM	0.918	0.926	0.952	0.934	0.923	0.926	**0.988**
	MS-SSIM	0.894	0.912	**0.943**	0.916	0.899	0.905	0.987
	VSI	0.960	0.971	0.988	0.982	0.976	0.977	**0.997**
	GMSD	0.106	0.087	0.032	0.045	0.063	0.056	**0.009**
Kangroo	AIC	6.787	6.858	6.590	6.889	6.847	6.846	**6.895**
	FSIM	0.859	0.881	0.831	0.913	0.864	0.880	**0.950**
	MS-SSIM	0.877	0.894	0.788	0.901	0.864	0.884	**0.944**
	VSI	0.946	0.957	0.932	0.965	0.949	0.955	**0.979**
	GMSD	0.106	0.082	0.100	0.030	0.076	0.066	**0.021**
Pyramid	AIC	6.200	6.309	5.972	6.340	6.287	6.306	**6.367**
	FSIM	0.890	0.885	0.697	0.906	0.819	0.832	**0.961**
	MS-SSIM	0.950	0.923	0.655	0.927	0.855	0.885	**0.969**
	VSI	0.976	0.972	0.908	0.978	0.954	0.957	**0.991**
	GMSD	0.080	0.070	0.175	0.049	0.111	0.108	**0.022**

Table 1 continued

Image	Metric	SSTHE 2009 [42]	DQHEPL 2010 [35]	MCDHB 2019 [37]	PLTHE 2018 [43]	TDCHEM 2018 [44]	TCDHESD 2019 [45]	Proposed
Family	AIC	5.600	5.752	5.579	5.810	5.765	5.770	**5.815**
	FSIM	0.909	0.937	0.951	0.973	0.939	0.952	**0.990**
	MS-SSIM	0.875	0.915	0.932	0.956	0.914	0.935	**0.986**
	VSI	0.971	0.977	0.990	0.992	0.978	0.982	**0.998**
	GMSD	0.100	0.082	0.070	0.032	0.070	0.053	**0.015**

Table 2 Performance evaluation of contrast enhancement algorithms

Image	Metric	SSTHE 2009 [42]	DQHEPL 2010 [35]	MCDHB 2019 [37]	PLTHE 2018 [43]	TDCHEM 2018 [44]	TCDHESD 2019 [45]	Proposed
Airplane	AIC	6.470	6.588	6.318	6.675	6.619	6.686	**6.700**
	FSIM	0.902	0.948	0.818	0.958	0.956	0.965	**0.971**
	MS-SSIM	0.916	0.954	0.794	0.963	0.952	0.962	**0.964**
	VSI	0.973	0.985	0.948	0.990	0.986	0.987	**0.994**
	GMSD	0.087	0.057	0.164	0.056	0.033	**0.023**	0.032
Kodim02	AIC	5.211	5.390	5.193	5.481	5.316	5.335	**5.516**
	FSIM	0.843	0.799	0.570	0.818	0.799	0.893	**0.951**
	MS-SSIM	0.868	0.805	0.398	0.830	0.890	0.912	**0.955**
	VSI	0.957	0.947	0.793	0.940	0.946	0.976	**0.988**
	GMSD	0.111	0.141	0.259	0.094	0.135	0.075	**0.027**
Dragonfly	AIC	6.176	6.330	6.011	6.363	6.275	6.317	**6.401**
	FSIM	0.918	0.876	0.668	0.932	0.858	0.877	**0.974**
	MS-SSIM	0.942	0.875	0.614	0.931	0.847	0.872	**0.972**
	VSI	0.973	0.958	0.887	0.980	0.952	0.960	**0.992**
	GMSD	0.071	0.086	0.192	0.040	0.088	0.90	**0.016**
Hills	AIC	6.667	6.739	6.600	6.785	6.771	6.778	**6.835**
	FSIM	0.855	0.929	0.890	0.949	0.962	0.955	**0.980**
	MS-SSIM	0.921	0.972	0.950	0.978	0.963	0.966	**0.988**
	VSI	0.958	0.983	0.967	0.989	0.992	0.991	**0.996**
	GMSD	0.077	0.035	0.057	0.023	0.024	0.032	**0.011**
Girl	AIC	7.122	7.213	7.093	7.238	7.207	7.206	**7.244**
	FSIM	0.938	0.964	0.959	0.965	0.950	0.954	**0.979**
	MS-SSIM	0.963	0.979	0.956	0.976	0.958	0.969	**0.982**
	VSI	0.981	0.990	0.987	0.990	0.986	0.987	**0.994**
	GMSD	0.067	0.034	0.048	0.030	0.044	0.037	**0.019**

(*Tiffany*, *Kodim02*, *Moon*, *Dragonfly*, *Girl*, *Airplane*, *Hawks*, *Hills*, *Buffalo*, *Lady*, *Child*, *Gate*, *Kangaroo*, *Pyramid*, and *Family*) are considered. Figure 5 is showing these test images, which are of diverse image features like different contrast and brightness from various well-known image data-sets ([51], [52], [53], [54]). The best result is shown in boldface, and the second best result is specified using underline for Tables 1, 2 and 3.

From Tables 1 and 2, it is clearly observed that the proposed method provides the best AIC values for all images except *Tiffany*, *Child* and *Gate* images, where the proposed method gives the second best result of AIC for *Tiffany* image. Proposed method offers the best FSIM and VSI results for all fifteen images. Suggested method delivers the highest MS-SSIM results for all images except *Moon*, *Tiffany*, and *Gate* images, where the next best values of MS-SSIM for these three images are given by the proposed method. Except *Child* and *Airplane* images, the proposed method demonstrates the best GMSD values for all images, where the second best

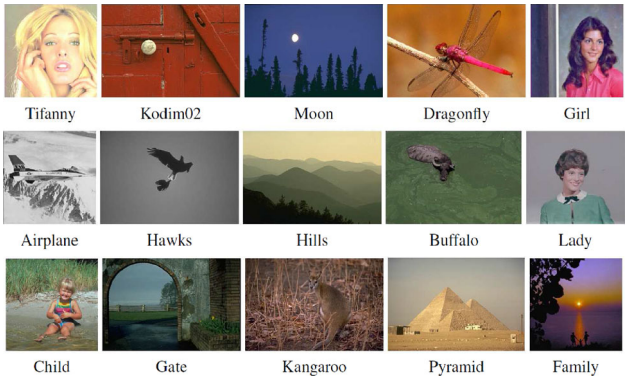

Fig. 5 Images from different data-sets for experimental analysis

value for *Child* and *Airplane* images are represented by the proposed method.

Box plot for different quantitative measures using different HE methods for various data-sets such as Kodak [52], CSIQ [53], Berkeley [54] is shown in Fig. 6, 7 and 8, respectively, where outcome of three best methods is marked as blue. It is observed that the proposed method provides superior performance with respect to the other techniques.

Table 3 illustrates average results of different quantitative metrics for various HE methods on different well-known image data-sets [52–54]. Here, except AIC metric of CSIQ [53] data-set, the proposed method shows the best performance for rest of the entities.

Table 4 represents the average computation time of various methods for different image data-sets (Kodak image data-set [52] (24 images of size 768 × 512 pixels), CSIQ image data-set [53] (30 images of size 512 × 512 pixels), Berkeley image data-set [54] (500 images of size 481 × 321 or 321 × 481 pixels)). Here, DQHEPL takes much higher time due to quad histogram separation, whereas MCDHB takes reasonably longer time due to multiple plateau limit operations. The suggested method is computationally capable, and it is appropriate for real-time applications.

3.2 Visual assessment

In visual assessment, seven test images (*Hawks*, *Buffalo*, *Kodim02*, *Moon*, *Hills*, *Airplane* and *Tiffany*) are taken into consideration from different image data-sets ([51], [52], [54]).

Figure 9 shows a low contrast *Hawks* image and output of different HE methods, where SSTHE provides an erroneous outcome in the middle of the image, and DQHEPL illustrates a little better output, but extra artifacts can be visible. MCDHB furnishes over-enhanced result with extra dark pixels. PLTHE does improve well, but a few pixels are washed out in the feather area of the large hawk as shown in the

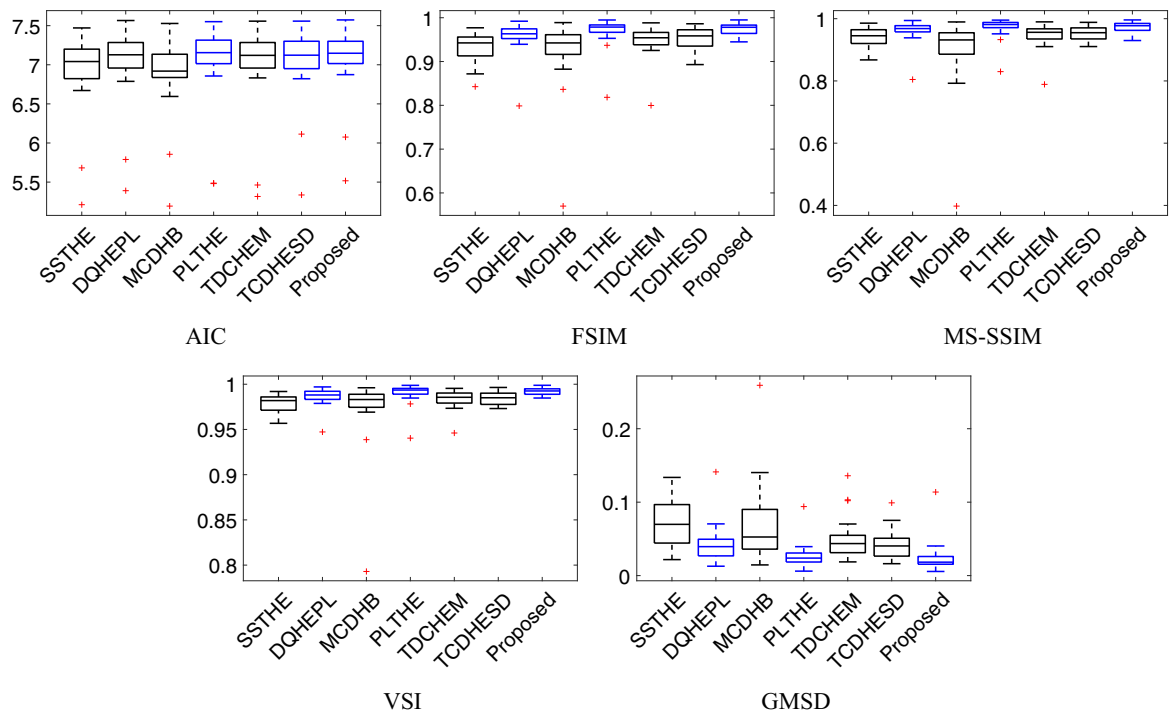

Fig. 6 Box plot for different quantitative measures using different HE methods for Kodak [52] data-set, where outcome of three best methods is marked as blue

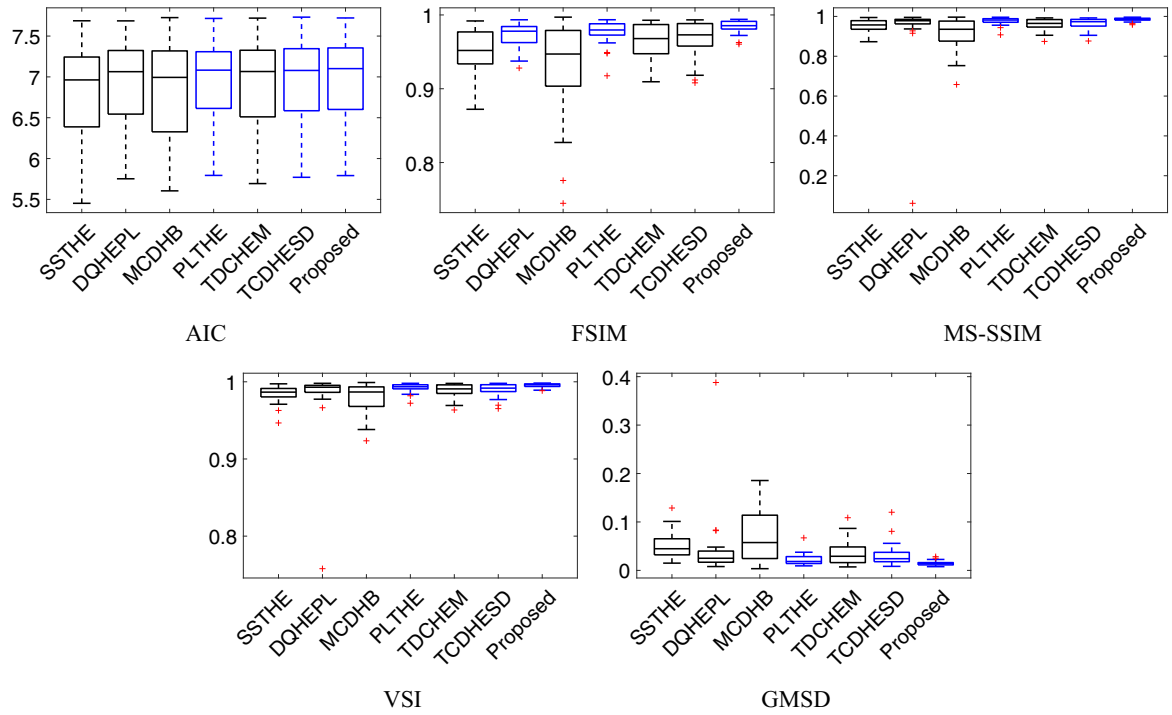

Fig. 7 Box plot for different quantitative measures using different HE methods for CSIQ [53] data-set, where outcome of three best methods is marked as blue

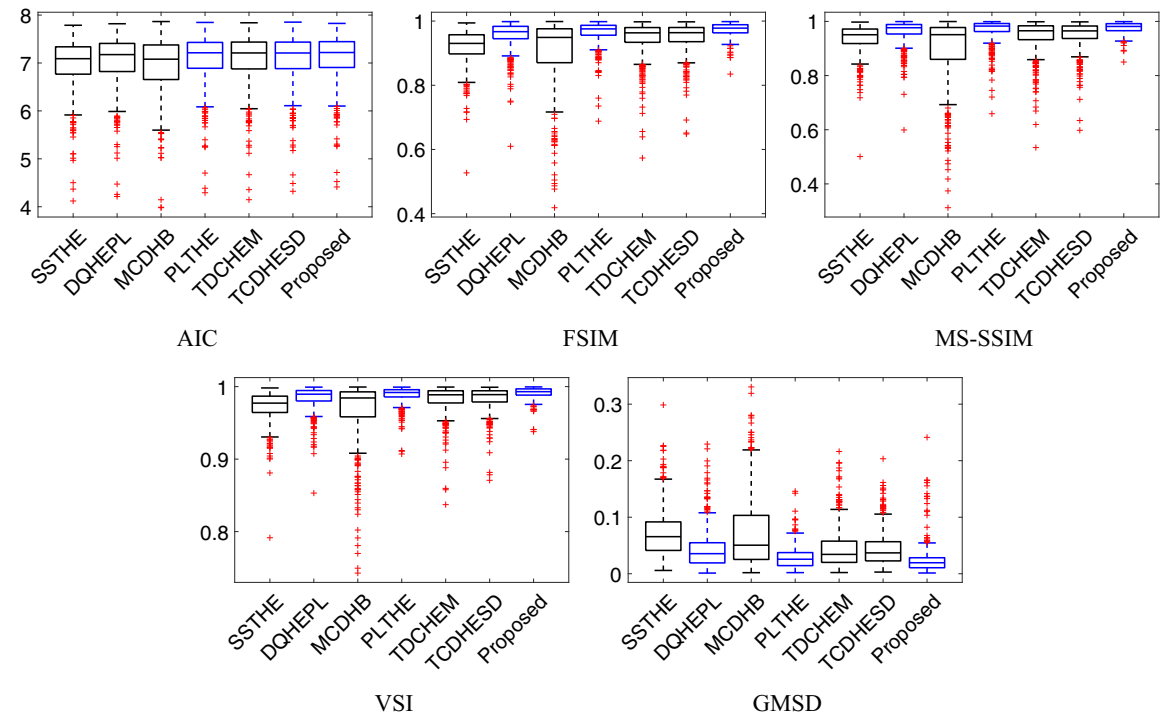

Fig. 8 Box plot for different quantitative measures using different HE methods for Berkeley [54] data-set , where outcome of three best methods is marked as blue

Table 3 Performance evaluation of various methods, where the average values of different quantitative metrics are shown for various image data-sets

Image data-set	Metric	SSTHE 2009 [42]	DQHEPL 2010 [35]	MCDHB 2019 [37]	PLTHE 2018 [43]	TDCHEM 2018 [44]	TCDHESD 2019 [45]	Proposed
Kodak	AIC	6.926	7.024	6.882	7.047	7.012	7.042	**7.068**
data-set [52]	FSIM	0.933	0.958	0.924	0.969	0.948	0.953	**0.974**
	MS-SSIM	0.939	0.961	0.903	0.972	0.947	0.954	**0.974**
	VSI	0.978	0.987	0.974	0.990	0.984	0.985	**0.992**
	GMSD	0.070	0.042	0.069	0.027	0.049	0.043	**0.024**
CSIQ	AIC	6.845	6.962	6.841	6.981	6.964	**6.986**	6.985
data-set [53]	FSIM	0.951	0.973	0.931	0.977	0.962	0.968	**0.984**
	MS-SSIM	0.9521	0.943	0.913	0.977	0.957	0.968	**0.985**
	VSI	0.984	0.983	0.979	0.992	0.988	0.989	**0.995**
	GMSD	0.051	0.045	0.069	0.023	0.035	0.032	**0.015**
Berkeley	AIC	6.975	7.046	6.941	7.089	7.082	7.087	**7.103**
data-set [54]	FSIM	0.920	0.956	0.908	0.966	0.947	0.951	**0.974**
	MS-SSIM	0.938	0.962	0.900	0.968	0.946	0.950	**0.977**
	VSI	0.972	0.984	0.967	0.988	0.983	0.984	**0.992**
	GMSD	0.072	0.042	0.073	0.028	0.044	0.043	**0.024**

Table 4 Average computational time (in sec) of various algorithms for different image data-sets

Image data-set	SSTHE 2009 [42]	DQHEPL 2010 [35]	MCDHB 2019 [37]	PLTHE 2018 [43]	TDCHEM 2018 [44]	TCDHESD 2019 [45]	Proposed
Kodak [52]	0.0749	0.1999	0.1641	0.0885	0.0729	0.1563	0.1393
CSIQ [53]	0.0672	0.0911	0.1172	0.0563	0.0443	0.0615	0.0896
Berkeley [54]	0.0232	0.0448	0.0574	0.0233	0.0240	0.0238	0.0332

cropped section. TDCHEM and TCDHESD supply almost alike output with some artifacts in the background region. Suggested scheme furnishes clear enhanced result with well-visualized background and foreground regions.

In Fig. 10, products of various HE methods are given for a slightly low contrast and dim *Buffalo* image, where SSTHE shows enhanced product with a few white and gloomy pixels. MCDHB gives over-enhanced output with a few extremely dark pixels. DQHEPL, TDCHEM, and TCDHESD give alike result with added dark pixels in the head region of the buffalo, but the water region is lightly well enhanced. PLTHE provides a well-enhanced outcome in most of the region of the image, but a few dark regions can be observed around the head area. Our recommended technique illustrates the best visualization concerning the other methods.

From the output results of various HE methods, as shown in Fig. 11, it is observed that our projected scheme not only restricts unwanted over-enhancement but also provides clear details with well-enhanced output concerning to the other methods.

For the *Moon* image, as shown in Fig. 12, SSTHE produces well-improved output with few artifacts in the middle region of the image. DQHEPL, TDCHEM, and TCDHESD give significantly better-enhanced outcome, but a few areas around the moon region get slightly over-enhanced. MCDHB algorithm offers over-enhanced result around the moon and sky regions. PLTHE can perform well but, minor pixels are washed-out around the moon region. The suggested scheme illustrates the best output with properly detailed enhancement.

Hills image and output of a diverse HE schemes are provided in Fig. 13, where SSTHE and DQHEPL present similar erroneous outcome, especially in the sky regions. MCDHB demonstrates extra dark pixels in the sky regions. PLTHE and TCDHESD give similar result with a few dark and erroneous pixels in the sky regions. TDCHEM shows dull and

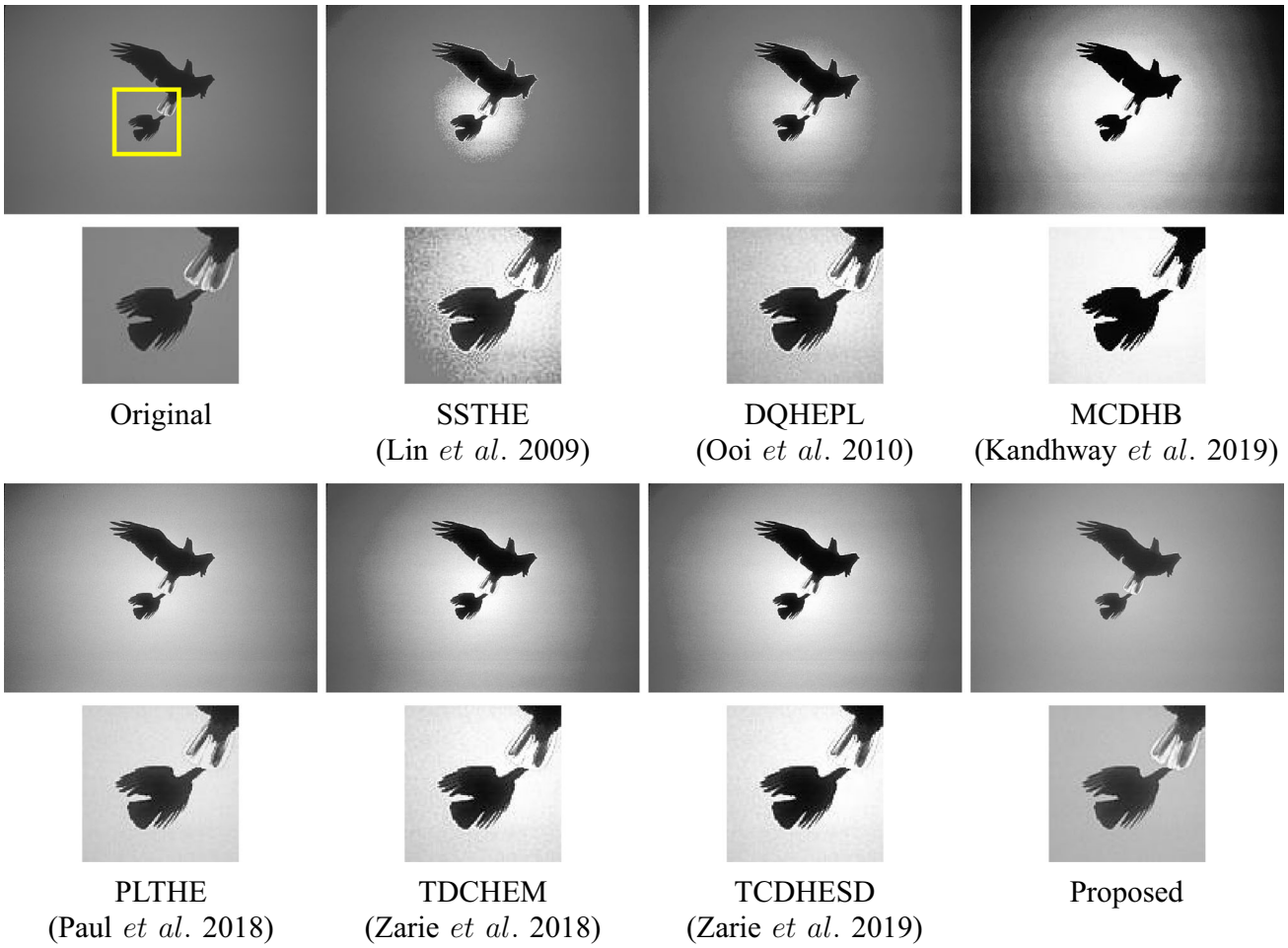

Fig. 9 *Hawks* image and output of SSTHE [42], DQHEPL [35], MCDHB [37], PLTHE [43], TDCHEM [44], TCDHESD [45], and Proposed method

low-contrast outcome. Our suggested technique produces the best product with clear visualization.

Figure 14 provides different results for the *Airplane* image. Here, SSTHE, TDCHEM, and TCDHESD present alike dull and low-contrast outcome. DQHEPL and PLTHE deliver similar result, where a few regions of plane and sky remain lightly dark. MCDHB provides extra dark regions and unwanted artifacts. Proposed method shows well-enhanced output, though few portion in the background get over-enhanced, but cropped section effectively justifies the superior outcome. Moreover, the histogram of output image is nicely distributed in dynamic intensity regions.

Figure 15 presents various HE outcomes of *Tiffany* image, where SSTHE gives extra dark pixels in the background region. DQHEPL, PLTHE, and TCDHESD show similar outcome, but few areas of head region remain dull and gloomy. MCDHB shows unwanted dark pixels over the whole region of the image. Background of TDCHEM is slightly over-enhanced with extra artifacts. Proposed scheme provides well-enhanced output with clear visualization with respect to the other methods.

A cropped portion is demonstrated for each image in Fig. 9, 10, 11, 12, 13, 14, 15. In Figs. 14 and 15, histogram of various HE methods is presented, where vertical axis indicates number of pixels and horizontal axis indicates image intensity. In Fig. 15, for each histogram, red, green, and blue color components are shown by red, blue, and green colors, respectively.

Figures 9, 10, 11, 12, 13, 14, 15 demonstrate visual representation of different HE methods for various images (*Hawks*, *Buffalo*, *Kodim02*, *Moon*, *Hills*, *Airplane* and *Tiffany*) considering YUV color space [60]. Apart from YUV color space, various other color spaces [21,56,60–62] are utilized in image enhancement techniques. HSV [21] color space is one of them. Here, an example of HSV color space using different HE methods for two images (*Girl* and *Hawks*)

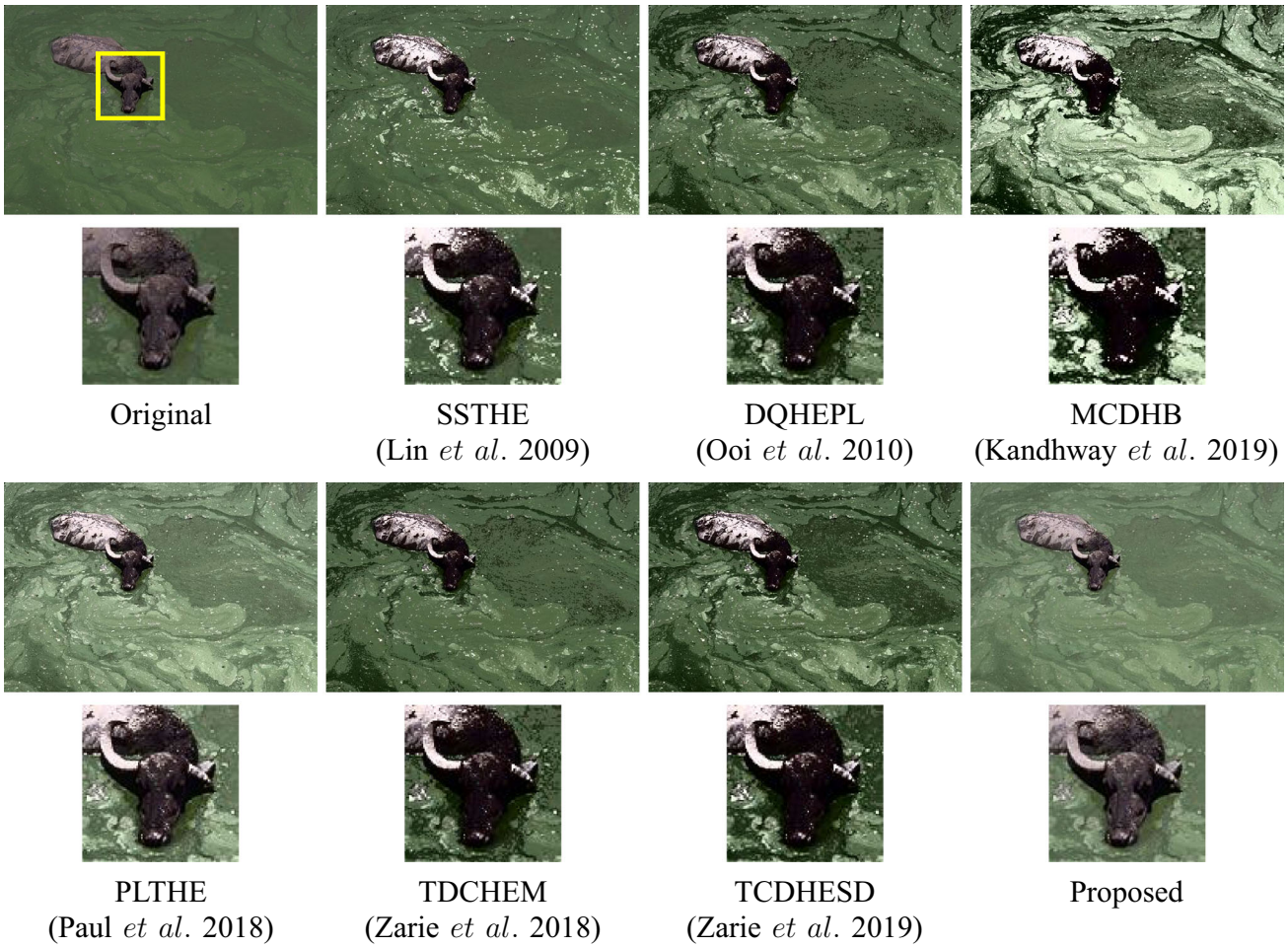

Fig. 10 *Buffalo* image and output of SSTHE [42], DQHEPL [35], MCDHB [37], PLTHE [43], TDCHEM [44], TCDHESD [45], and Proposed method

are shown in Fig. 16. Here, SSTHE and DQHEPL perform well, but MCDHB, TDCHEM, and TCDHESD provide extra artifacts. PLTHE provide comparatively well-enhanced output. The proposed method provides the best outcome comparing other techniques.

Visual outcomes and quantitative results positively authenticate the superiority of the suggested technique; however, our proposed technique would be extended by establishing a parallel processing technology to minimize the computational time.

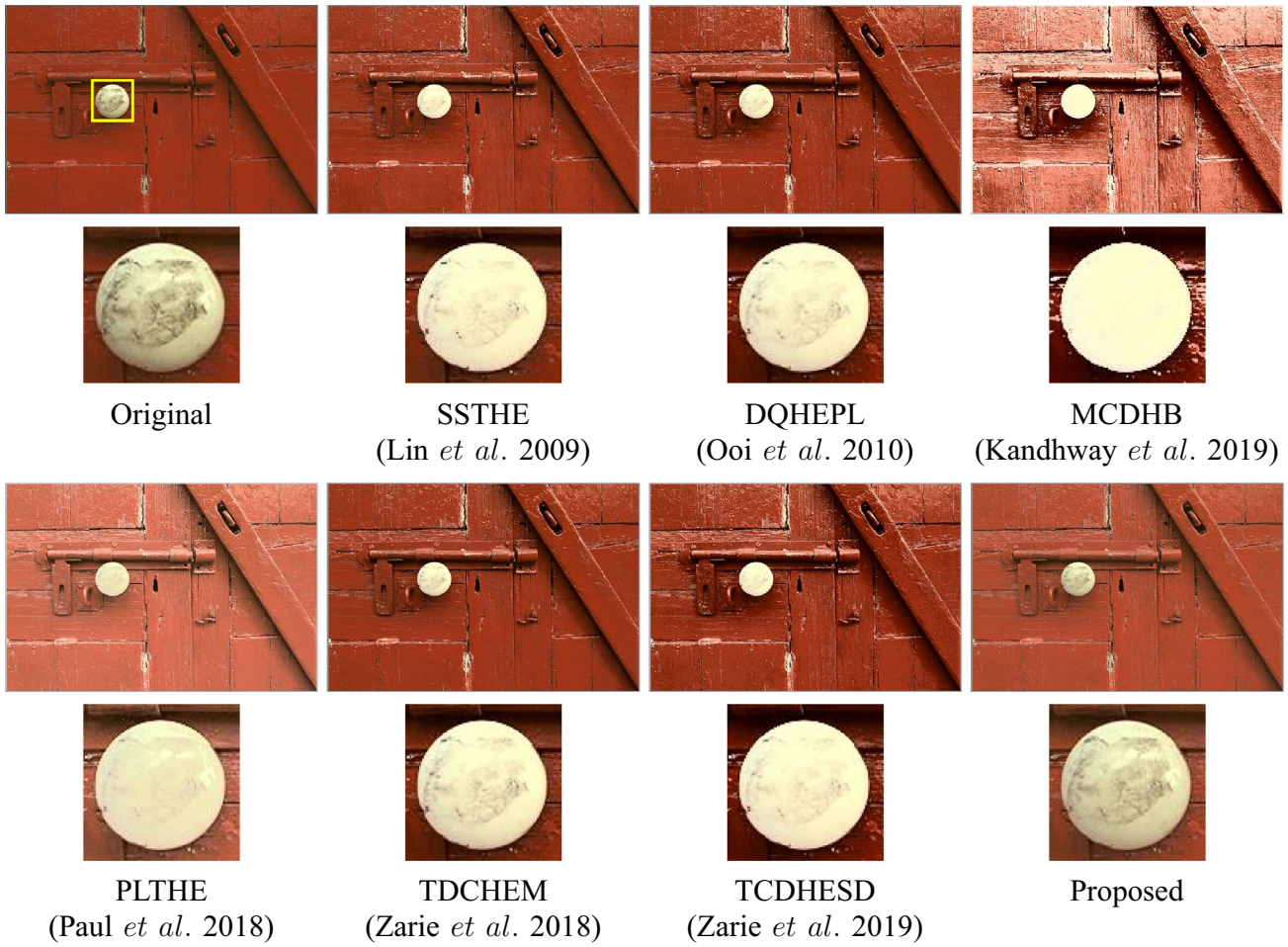

Fig. 11 *Kodim02* image and output of SSTHE [42], DQHEPL [35], MCDHB [37], PLTHE [43], TDCHEM [44], TCDHESD [45], and Proposed method

4 Conclusions

In this paper, a novel adaptive tri-plateau limit tri-histogram equalization technique is suggested for digital image enhancement, where input histogram is split in three sub-histograms, and subsequently each sub-histogram is clipped and modified using redistribution parameter, and finally, each modified sub-histogram is equalized individually. Recent improved algorithms like SSTHE, DQHEPL, MCDHB, PLTHE, TCDHEM, and TCDHESD are compared with the proposed approach. Quantitative metrics like AIC, FSIM, MS-SSIM, VSI, and GMSD are utilized for comparative assessment; in addition, three well-known image data-sets are considered for various quantitative outcomes of different HE methods and illustrated in graph plots, which depicts the superior result of our proposed technique. Moreover, the visual output of the suggested method gives superior clear visualization concerning the other state-of-the-art methods.

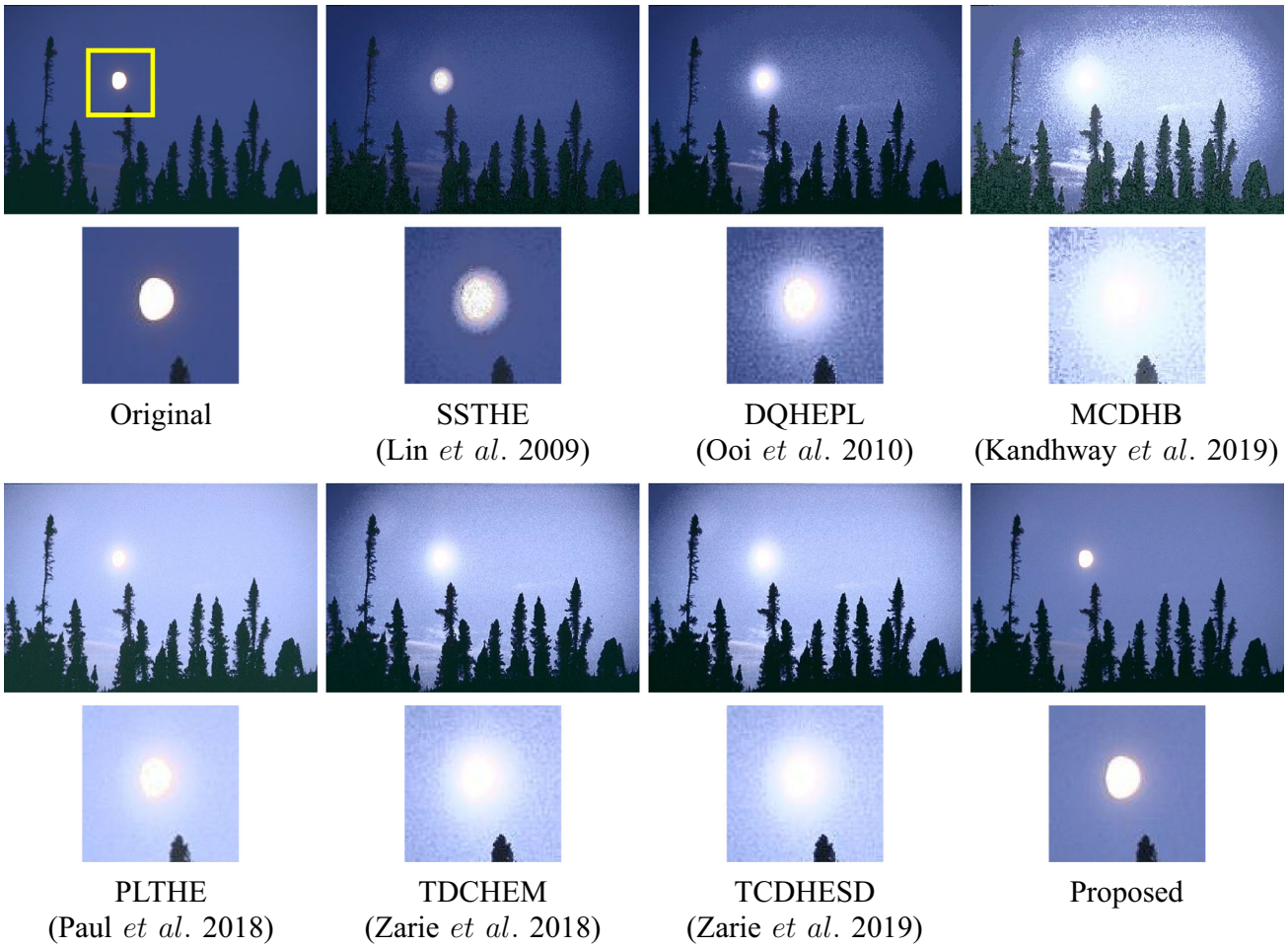

Fig. 12 *Moon* image and output of SSTHE [42], DQHEPL [35], MCDHB [37], PLTHE [43], TDCHEM [44], TCDHESD [45], and Proposed method

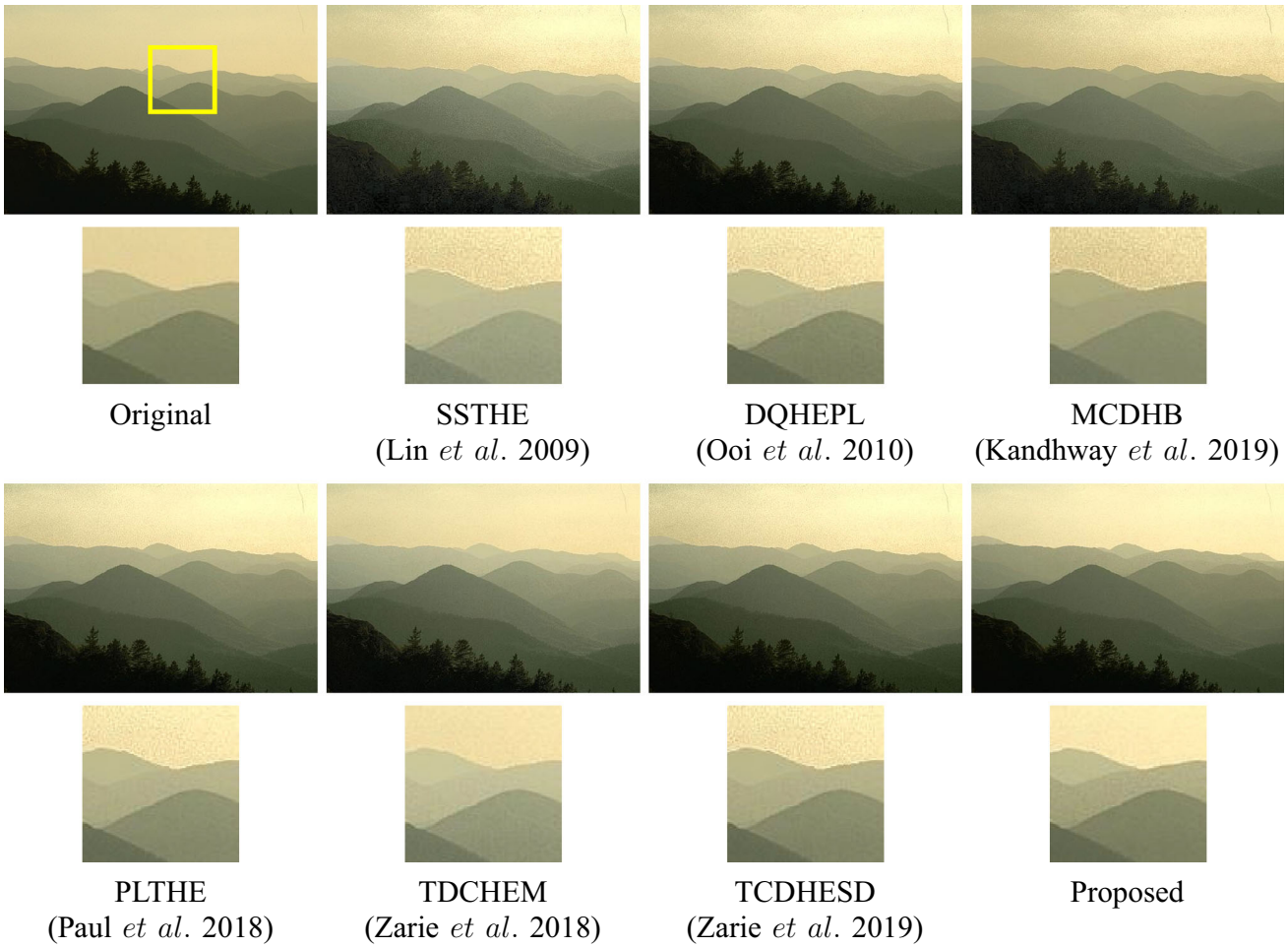

Fig. 13 *Hills* image and output of SSTHE [42], DQHEPL [35], MCDHB [37], PLTHE [43], TDCHEM [44], TCDHESD [45], and Proposed method

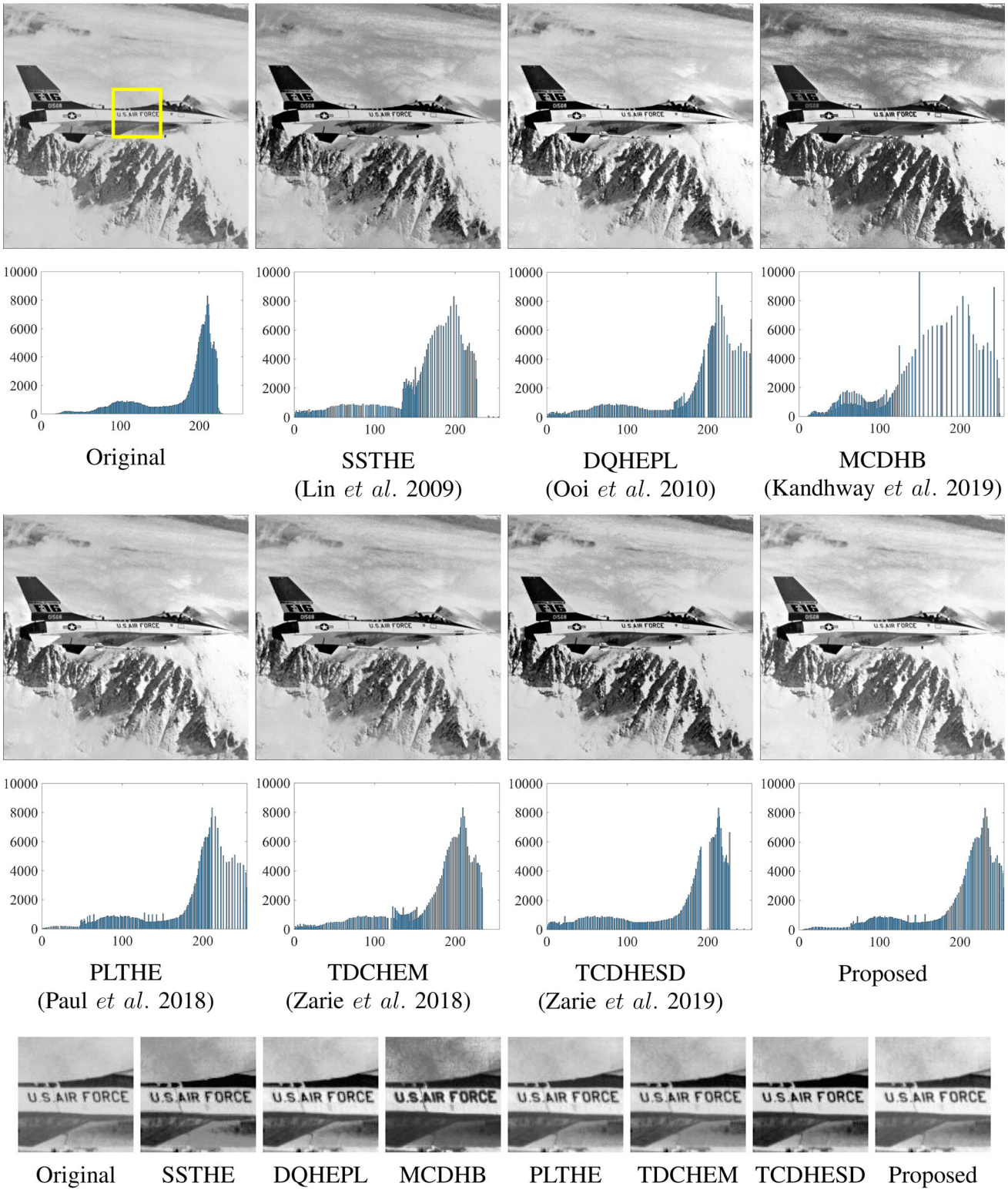

Fig. 14 *Airplane* image and output of SSTHE [42], DQHEPL [35], MCDHB [37], PLTHE [43], TDCHEM [44], TCDHESD [45], and Proposed method

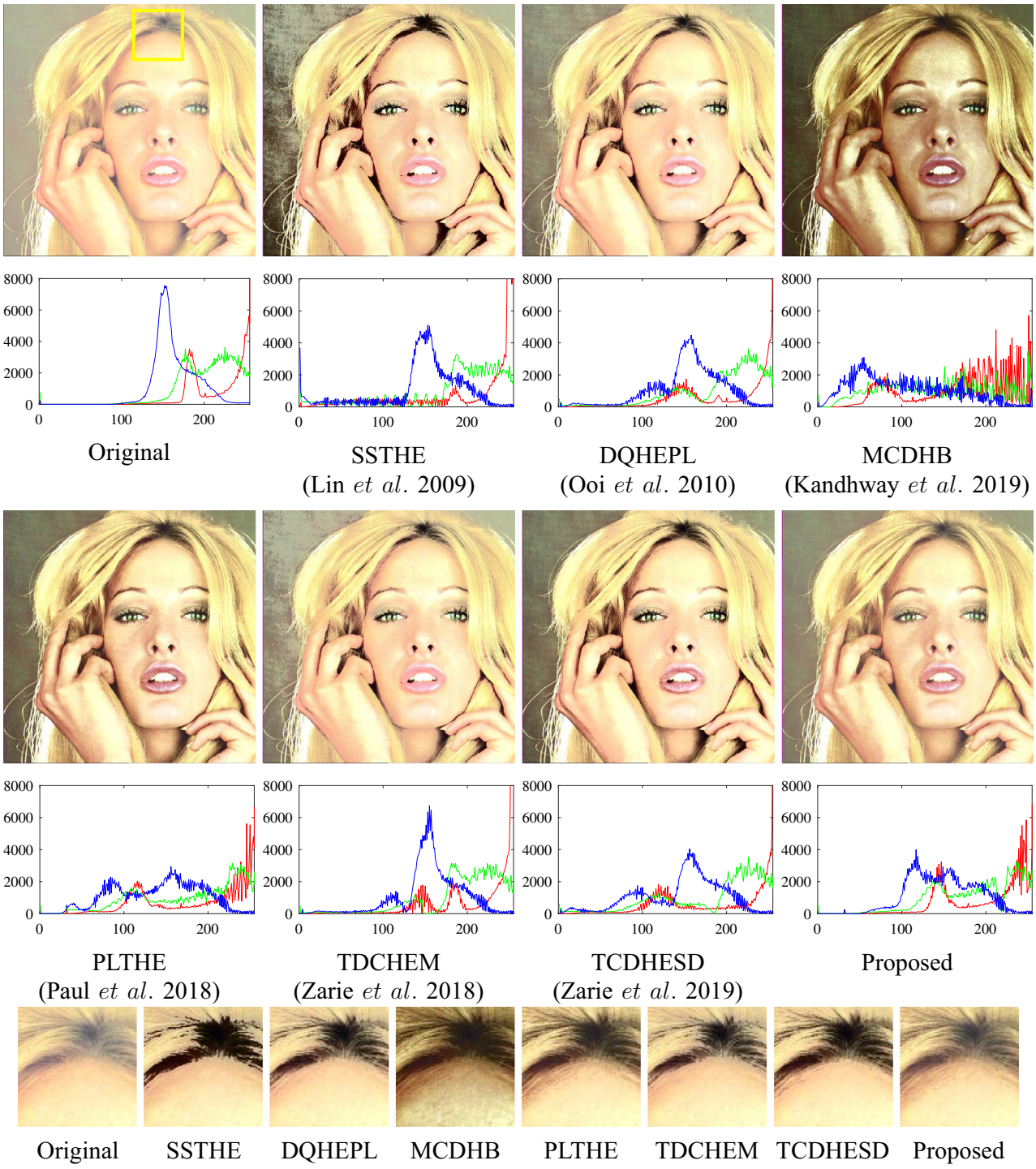

Fig. 15 *Tiffany* image and output of SSTHE [42], DQHEPL [35], MCDHB [37], PLTHE [43], TDCHEM [44], TCDHESD [45], and Proposed method

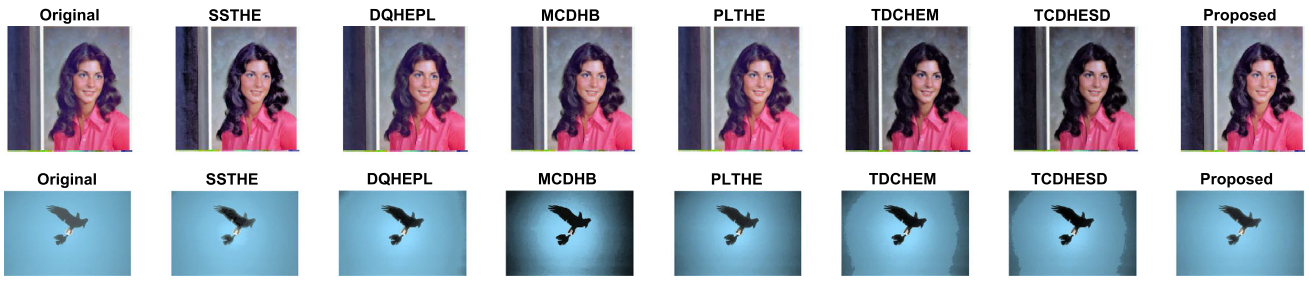

Fig. 16 Output of different HE methods using HSV color space for *Tiffany* image (first row) and *Hawks* image (second row)

References

1. Loh, Y.P., Liang, X., Chan, C.S.: Low-light image enhancement using Gaussian Process for features retrieval. Signal Process. Image Commun. **74**, 175–190 (2019)
2. Chang, S., Cai, X., Flueraru, C.: Image enhancement for multilayer information retrieval by using full-field optical coherence tomography. Appl. Opt. **45**(23), 5967–5975 (2006)
3. Iqbal, K., Odetayo, M., James, A., Iqbal, R., Kumar, N., Barma, S.: An efficient image retrieval scheme for colour enhancement of embedded and distributed surveillance images. Neurocomputing **174**, 413–430 (2016)
4. Jin, C., Luan, N.: An image denoising iterative approach based on total variation and weighting function. Multimed. Tools Appl. **79**(29), 20947–20971 (2020)
5. Zhang, S., He, F., Ren, W., Yao, J.: Joint learning of image detail and transmission map for single image dehazing. The Vis. Comput. **36**(2), 305–316 (2020)
6. Raikwar, S.C., Tapaswi, S.: Tight lower bound on transmission for single image dehazing. The Vis. Comput. **36**(1), 191–209 (2020)
7. Chen, Z., Hu, Z., Sheng, B., Li, P., Kim, J., Wu, E.: Simplified non-locally dense network for single-image dehazing. The Vis. Comput. **36**(10), 2189–2200 (2020)
8. Moriyama, D., Azetsu, T., Ueda, C., Suetake, N., Uchino, E.: Image enhancement with lightness correction and image sharpening based on characteristics of vision for elderly persons. Opt. Rev. **27**, 352–360 (2020)
9. Dawood, H., Dawood, H., Ping, G., Mehmood, R., Daud, A., Alamri, A., et al.: Probability weighted moments regularization based blind image De-blurring. Multimed. Tools Appl. **79**(7), 4483–4498 (2020)
10. Das, B., Ebenezer, J.P., Mukhopadhyay, S.: A comparative study of single image fog removal methods. The Visual Computer. **1–17**,(2020)
11. Anwar, S., Rajamohan, G.: Improved image enhancement algorithms based on the switching median filtering technique. Arab. J. Sci. Eng. **45**(12), 11103–11114 (2020)
12. Cao, L., Li, H.: Enhancement of blurry retinal image based on non-uniform contrast stretching and intensity transfer. Med. Biol. Eng. Comput. **58**(3), 483–496 (2020)
13. Zhang, L., Yan, Q., Zhu, Y., Zhang, X., Xiao, C.: Effective shadow removal via multi-scale image decomposition. The Vis. Comput. **35**(6), 1091–1104 (2019)
14. Tang, Y., Sun, J., Jiang, A., Chen, Y., Zhou, L.: Adaptive graph filtering with intra-patch pixel smoothing for image denoising. Circuit. Syst. Sig. Process. 1–20 (2021)
15. Chen, L., Fu, G.: Structure-preserving image smoothing with semantic cues. The Vis. Comput. **36**(10), 2017–2027 (2020)
16. Gonzalez, R.C., Woods, R.E., et al.: Digital image processing. Prentice hall Upper Saddle River, NJ (2002)
17. Gandhi, C. R., Murugesh, V.: A contrast adaptive histogram equalization with neural learning quantization (CAHE-NLQ) for blood clot detection in brain. J. Ambient Intell. Human. Comput. 1–15 (2021)
18. Sirajuddeen, C., Kansal, S., Tripathi, R.K.: Adaptive histogram equalization based on modified probability density function and expected value of image intensity. Sig. Image Video Process. **14**(1), 9–17 (2020)
19. Joshi, P., Prakash, S.: Image enhancement with naturalness preservation. The Vis. Comput. **36**(1), 71–83 (2020)
20. Bulut, F.: Low dynamic range histogram equalization (LDR-HE) via quantized Haar wavelet transform. The Vis. Comput. 1–17 (2021)
21. Ulutas, G., Ustubioglu, B.: Underwater image enhancement using contrast limited adaptive histogram equalization and layered difference representation. Multimed. Tools Appl. 1–25 (2021)
22. Paul, A., Sutradhar, T., Bhattacharya, P., Maity, S.P.: Adaptive clip-limit-based bi-histogram equalization algorithm for infrared image enhancement. Appl. Opt. **59**(28), 9032–9041 (2020)
23. Paul, A., Sutradhar, T., Bhattacharya, P., Maity, S.P.: Infrared images enhancement using fuzzy dissimilarity histogram equalization. Optik. 167887 (2021)
24. Simi, V., Edla, D.R., Joseph, J., Kuppili, V.: Parameter-free fuzzy histogram equalisation with illumination preserving characteristics dedicated for contrast enhancement of magnetic resonance images. Appl. Soft Comput. **93**, 106364 (2020)
25. Siddiqi, A.A., Narejo, G.B., Tariq, M., Hashmi, A.: Investigation of histogram equalization filter for CT scan image enhancement. Biomed. Eng. Appl. Basis Commun. **31**(05), 1950038 (2019)
26. Sidar, I., Davidson, T., Kronman, A., Lior,. M., Levy, I.: Endoscopic image enhancement using contrast limited adaptive histogram equalization (clahe) implemented in a processor. Google Patents. US Patent App. 16/685,299 (2020)
27. Rong, Z., Li, Z., Dong-nan, L.: Study of color heritage image enhancement algorithms based on histogram equalization. Optik **126**(24), 5665–5667 (2015)
28. Singh, H., Kumar, A., Balyan, L., Lee, H.: Optimally sectioned and successively reconstructed histogram sub-equalization based gamma correction for satellite image enhancement. Multimed. Tools Appl. **78**(14), 20431–20463 (2019)
29. Kim, Y.T.: Contrast enhancement using brightness preserving bi-histogram equalization. IEEE Trans. Cons. Electron. **43**(1), 1–8 (1997)
30. Wang, Y., Chen, Q., Zhang, B.: Image enhancement based on equal area dualistic sub-image histogram equalization method. IEEE Trans. Cons. Electron. **45**(1), 68–75 (1999)
31. Chen, S.D., Ramli, A.R.: Minimum mean brightness error bi-histogram equalization in contrast enhancement. IEEE Trans. Cons. Electron. **49**(4), 1310–1319 (2003)
32. Chen, S.D., Ramli, A.R.: Contrast enhancement using recursive mean-separate histogram equalization for scalable bright-

ness preservation. IEEE Trans. Cons. Electron. **49**(4), 1301–1309 (2003)
33. Sim, K., Tso, C., Tan, Y.: Recursive sub-image histogram equalization applied to gray scale images. Pattern Recog. Lett. **28**(10), 1209–1221 (2007)
34. Ooi, C.H., Kong, N.S.P., Ibrahim, H.: Bi-histogram equalization with a plateau limit for digital image enhancement. IEEE Trans. Cons. Electron. **55**(4), 2072–2080 (2009)
35. Ooi, C.H., Isa, N.A.M.: Adaptive contrast enhancement methods with brightness preserving. IEEE Trans. Cons. Electron. **56**(4), 2543–2551 (2010)
36. Aquino-Morínigo, P.B., Lugo-Solís, F.R., Pinto-Roa, D.P., Ayala, H.L., Noguera, J.L.V.: Bi-histogram equalization using two plateau limits. Sig. Image Video Process. **11**(5), 857–864 (2017)
37. Kandhway, P., Bhandari, A.K.: Modified clipping based image enhancement scheme using difference of histogram bins. IET Image Process. **13**(10), 1658–1670 (2019)
38. Huang, Z., Wang, Z., Zhang, J., Li, Q., Shi, Y.: Image enhancement with the preservation of brightness and structures by employing contrast limited dynamic quadri-histogram equalization. Optik **226**, 165877 (2021)
39. Pineda, I.A.B., Caballero, R.D.M., Silva, J.J.C., Román, J.C.M., Noguera, J.L.V.: Quadri-histogram equalization using cutoff limits based on the size of each histogram with preservation of average brightness. Sig. Image Video Process. **13**(5), 843–851 (2019)
40. Caballero, R.D.M., Pineda, I.A.B., Román, J.C.M., Noguera, J.L.V., Silva, J.J.C.: Quadri-Histogram Equalization for infrared images using cut-off limits based on the size of each histogram. Infrared Phys. Technol. **99**, 257–264 (2019)
41. Qadar, M.A., Zhaowen, Y., Rehman, A., Alvi, M.A.: Recursive weighted multi-plateau histogram equalization for image enhancement. Optik **126**(24), 5890–5898 (2015)
42. Lin, P.H., Lin, C.C., Yen, H.C., Tri-histogram equalization based on first order statistics. In: IEEE 13th International Symposium on Consumer Electronics. IEEE **2009**, 387–391 (2009)
43. Paul, A., Bhattacharya, P., Maity, S.P., Bhattacharyya, B.K.: Plateau limit-based tri-histogram equalisation for image enhancement. IET Image Process. **12**(9), 1617–1625 (2018)
44. Zarie, M., Hajghassem, H., Majd, A.E.: Contrast enhancement using triple dynamic clipped histogram equalization based on mean or median. Optik **175**, 126–137 (2018)
45. Zarie, M., Pourmohammad, A., Hajghassem, H.: Image contrast enhancement using triple clipped dynamic histogram equalisation based on standard deviation. IET Image Process. **13**(7), 1081–1089 (2019)
46. Shannon, C.E.: A mathematical theory of communication. Bell Syst. Tech. J. **27**(3), 379–423 (1948)
47. Zhang, L., Zhang, L., Mou, X., Zhang, D.: FSIM: a feature similarity index for image quality assessment. IEEE Trans. Image Process. **20**(8), 2378–2386 (2011)
48. Wang Z, Simoncelli EP, Bovik AC. Multiscale structural similarity for image quality assessment. In: The Thrity-Seventh Asilomar Conference on Signals, Systems & Computers, **2**, 1398–1402 (2003)
49. Zhang, L., Shen, Y., Li, H.: VSI: a visual saliency-induced index for perceptual image quality assessment. IEEE Trans. Image Process. **23**(10), 4270–4281 (2014)
50. Xue, W., Zhang, L., Mou, X., Bovik, A.C.: Gradient magnitude similarity deviation: a highly efficient perceptual image quality index. IEEE Trans. Image Process. **23**(2), 684–695 (2013)
51. Signal and Image Processing Institute of USC University of Southern California. The USC-SIPI image database;. Accessed January 4, 2020. [On-line]. Available: http://sipi.usc.edu/database/database.php
52. Franzen, R.: Kodak lossless true color image suite. Accessed January 4, 2020. [On-line]. Available: http://r0k.us/graphics/kodak/
53. Larson, E.C., Chandler, D.M.: Most apparent distortion: full-reference image quality assessment and the role of strategy. J. Electron. Imag. **19**(1), 011006 (2010)
54. The Berkeley Segmentation Dataset and Benchmark;. Accessed January 4, 2020. [On-line]. Available: https://www2.eecs.berkeley.edu/Research/Projects/CS/vision/bsds/
55. Liu, X.: Total generalized variation and wavelet frame-based adaptive image restoration algorithm. The Vis. Comput. **35**(12), 1883–1894 (2019)
56. Bhandari, A.K.: A logarithmic law based histogram modification scheme for naturalness image contrast enhancement. J. Ambient Intell. Human. Comput. **11**(4), 1605–1627 (2020)
57. Yuan, Q., Li, J., Zhang, L., Wu, Z., Liu, G.: Blind motion deblurring with cycle generative adversarial networks. The Vis. Comput. **36**(8), 1591–1601 (2020)
58. Srinivas, K., Bhandari, A.K., Singh, A.: Exposure-based energy curve equalization for enhancement of contrast distorted images. IEEE Trans. Circuit Syst. Video Technol. **30**(12), 4663–4675 (2019)
59. Acharya, U.K., Kumar, S.: Particle swarm optimized texture based histogram equalization (PSOTHE) for MRI brain image enhancement. Optik **224**, 165760 (2020)
60. Gao, G., Lai, H., Liu, Y., Wang, L., Jia, Z.: Sandstorm image enhancement based on YUV space. Optik **226**, 165659 (2021)
61. Zhang, S., Wang, T., Dong, J., Yu, H.: Underwater image enhancement via extended multi-scale Retinex. Neurocomputing **245**, 1–9 (2017)
62. Wang, P., Wang, Z., Lv, D., Zhang, C., Wang, Y.: Low illumination color image enhancement based on Gabor filtering and Retinex theory. Multimed. Tools Appl. **80**(12), 17705–17719 (2021)

Abhisek Paul received his PhD degree from the Department of Computer Science and Engineering, National Institute of Technology Agartala, India. He received his masters degree from the Department of Computer Science and Engineering, Tripura University (Central University). His research interests include digital image processing, soft computing, and artificial intelligence.